


 Cite this: *RSC Adv.*, 2023, **13**, 23396

Coordination-directed self-assembly of nano-cages: metal ion-change, ligand-extending, shape-control and transdermal drug delivery†

 Ying Zhang,^b Chi-Yu Sun ^a and Lin Lin ^{*a}

The combination of different pyridyl ligands and metal ions has proven to be a very reliable strategy for controlling the coordination mode of the heterometallic coordination nano-cages. Adjusting the length of the ligands could result in the selective synthesis of several heterometallic coordination nano-cages, either [8Rh + 2M]-4L, [8Rh + 2M]-5L or [8Rh + 4M]-6L cages, derived from the very same precursors (LH₃tzdc) through half-sandwich rhodium self-assembly. Moreover, a series of [8Rh + 4M]-6L cages was chosen to exemplify the preparation. The rigidity of various pyridyl donor ligands caused the vertical nano-cage to be energetically preferred and was able to change the self-assembly process through ligand flexibility to selectively give the inclined nano-cage and cross nano-cage.

Received 20th June 2023

Accepted 19th July 2023

DOI: 10.1039/d3ra04150f

rsc.li/rsc-advances

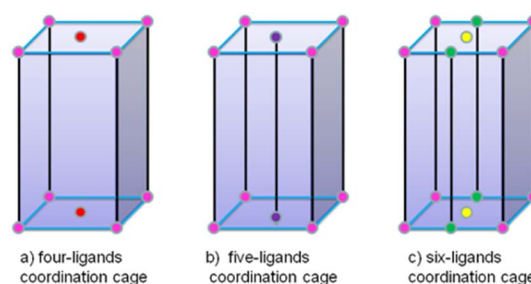
1. Introduction

Over the past two decades, coordination-driven self-assembly has developed into an efficient way to construct diverse metal-organic metallacycles and nano-cages with well-defined shapes, sizes and applications.^{1–5} The structural outcomes of metallasupramolecular self-assembly processes are largely controlled by factors such as the building blocks, metal ions, and organic ligands.⁶ By choosing an appropriate ligand, it is possible to influence the size, geometry, and functionality of the resulting metallasupramolecular assembly. Heterometallic coordination complexes have attracted considerable attention due to their aesthetically pleasing structures and also their potential applications in catalysis, electronic, magnetic, host-guest, drug delivery and other fields.^{7–10} However, the construction of well-defined metallasupramolecular coordination complexes, especially stable large structures, presents a challenge because changing the metal ions or an increase in linker length may lead to an increase in structure flexibility and multiple stereochemical configurations. Therefore, the use of different metal ions and ligands to control the assembly of metallasupramolecular coordination complexes is a well-established methodology.

The metal centers can be an extremely important consideration when designing heterometallic assemblies and represent

a significant advantage. Supramolecular chemistry based on Cp^{*}M (M = Ir, Rh) and (*p*-cymene) Ru units has grown rapidly since the first report of the organometallic Cp^{*}Rh fragment being used as a building block for the construction of discrete heterometallic architectures with metal acceptor units and nitrogen donor ligands.^{11,12} The coordination of pyridyl-based ligands with Cp^{*}Rh or Cp^{*}Ir fragments has proven very useful for constructing a wide array of metallamacrocycles, which has enabled the construction of a variety of metal-organic cages.^{13–22}

In our previous work, structures ranging from a one-dimensional (1D) organometallic chain up to 3D discrete heterometallic nano-cages have been constructed from half-sandwich Cp^{*}Rh units with triazole proligand 1,2,3-triazole-4,5-dicarboxylate (LH₃tzdc) and linear N-donor ligands of different lengths.^{23–33} Scheme 1 shows the design and self-assembly of discrete coordination cages based on three modes. The rigid ligands are a prerequisite for the assembly of four-ligand coordination nano-cages and flexible ligands tend to favor diverse



Scheme 1 The three modes of self-assembly of heterometallic coordination cages observed in this work, with different metal centers and ligands (pink for Rh, red for Zn, Ni, or Na; purple for Zn or Ni; yellow for Na or K, green for Cu).

^aDepartment of Translational Medicine Research Centre, School of Pharmacy, Shenyang Medical College, Shenyang 110034, China. E-mail: linlin1986@symc.edu.cn

^bThe Key Laboratory of the Inorganic Molecule-Based Chemistry of Liaoning Province and Laboratory of Coordination Chemistry, Shenyang University of Chemical Technology, Shenyang 110142, China. E-mail: zhangy621@syuct.edu.cn

† CCDC 1–5: 1 (1483412), 2 (1483419), 3 (1483405), 4 (1493420) and 5 (1483409) contain the supplementary X-ray single-crystal diffraction data for this paper. For crystallographic data in CIF or other electronic format see DOI: <https://doi.org/10.1039/d3ra04150f>



complexes of five-ligand coordination nano-cages. On changing the center metal ions, it is also possible to influence the metal nuclearity, quantity of ligands and the resulting six-ligand coordination mode of the assemblies. Therefore, the strategic

adjustment of the length of the pyridyl donor ligands and changing the metal center ions allowed us to control the self-assembly behavior of the systems.^{34–39} Transdermal drug delivery systems (TDDSs) are an innovative approach for delivering drugs into the blood at a controlled rate *via* the skin. TDDSs avoid the first-pass effect and improve patient compliance because they are applied topically. Heterometallic cage compounds are expected to be outstanding TDDS materials but to the best of our knowledge, such materials have yet to be reported in the literature. However, the construction of well-defined metalla-supramolecular coordination complexes, especially stable larger structures, presents a challenge because changing the metal ions or increasing the linker length may lead to an increase in the structural flexibility and multiple stereochemical configurations. Therefore, the use of different metal ions and ligands to control the assembly of metallocsupramolecular coordination complexes is a well-established methodology (Fig. 1).

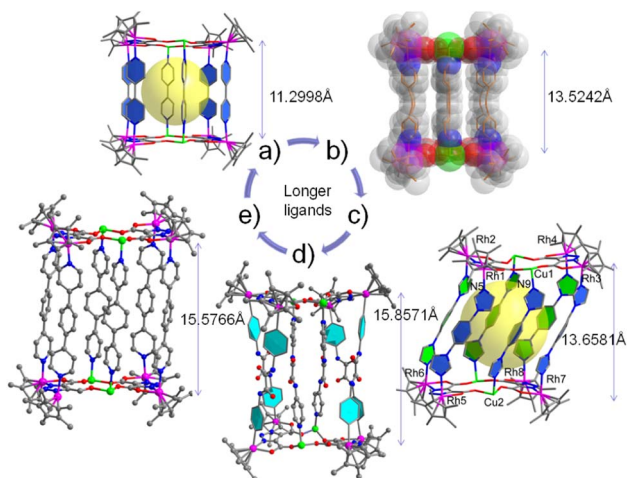
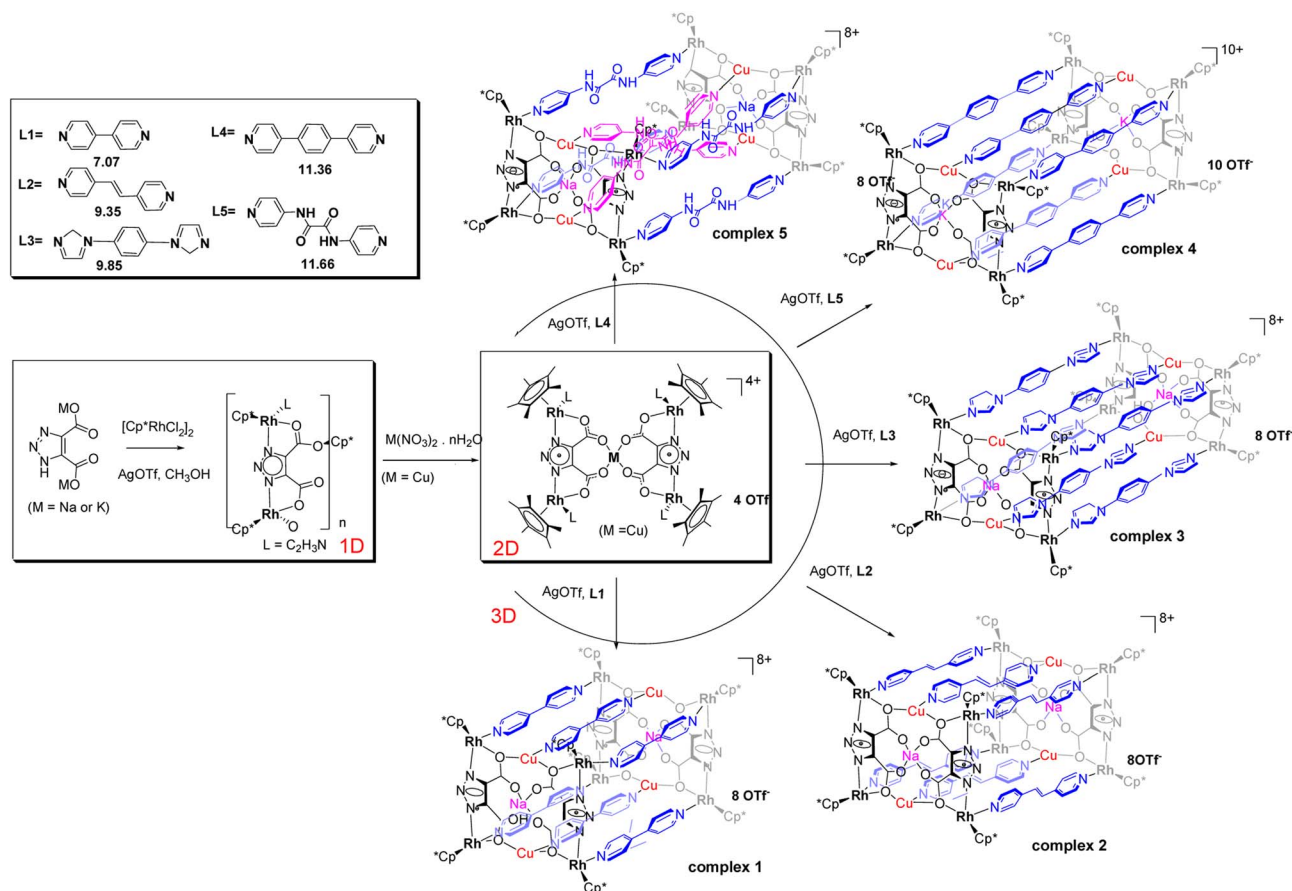


Fig. 1 (a)–(e) Single-crystal structures of 1–5 (gray for C, blue for N, red for O, green for Cu, pink for Rh, orange for Na, yellow for S, fluorescent green for F; Na some hydrogen atoms and solvent molecules or anions are omitted for clarity).

2. Results and discussion

As shown in Scheme 2, a variety of supramolecular coordination assemblies, from a 1D chain structure to 2D ($M = \text{Cu}$) polygons and 3D ($M = \text{Cu}, \text{Na}$) nano-cages, have been constructed by using metal ions to tune their cage sizes for potential applications.^{40–51} The sodium or potassium salt of LH3tzdc was added to a solution



Scheme 2 The synthetic routes to 1D chain structures, 2D polygons and 3D nano-cages.



of $[\text{Cp}^*\text{RhCl}_2]_2$ in MeOH. The reaction mixture was stirred with AgOTf for 12 h, and then sixfold pyridyl donor ligands (L1 to L5) with the metal salt $\text{Cu}(\text{NO}_3)_2 \cdot 3\text{H}_2\text{O}$ were added to the mixture, and five kinds of $[\text{8Rh} + 4\text{Cu}]_6\text{L}$ cages were obtained respectively. In such an assembly process, it is crucial to select appropriate metal ions that can be linked by the ligands. Cu–O linkages are more flexible and have versatile coordination behavior and favorable hard–soft combination. A variety of heteroleptic complexes 1–5 nano-cages were generated from the combination of sixfold pyridyl donor ligands. In Fig. 2a, the vertical nano-cage of complex 1 consists of eight Cp^*Rh fragments at the corners, and the two pairs of $[\text{4Rh} + 2\text{Cu}]$ units are bridged with sixfold L1. Each $[\text{4Rh} + 2\text{Cu}]$ unit is formed by two $\text{Cu}(\text{II})$ ions and four Cp^*Rh units, which are chelated by two LHTzdc units. By utilizing LHTzdc-based units that coordinate with $\text{Cu}(\text{II})$ ions as building blocks, we have synthesized the nano-cage complex 2 in Fig. 2b, displaying a $\text{Rh1A} \cdots \text{Rh1B}$ distance of 13.5242(4) Å, $\text{Na1A} \cdots \text{Na1B}$ distance of 13.3227(7) Å and a $\text{Cu1A} \cdots \text{Cu1B}$ distance of 13.4794(4) Å. The nano-cage of complex 1 is quite similar to that of complex 2 and has a cuboid cavity with dimensions of $6.19 \times 11.21 \times 10.48$ Å according to $\text{Rh} \cdots \text{Rh}$ non-bonding distances, which is much larger than that of complex 9 $6.20 \times 13.52 \times 10.40$ Å. Complexes 3 (Fig. 2c) and 4 (Fig. 2d) are inclined cuboid nano-cages with six L3 or L4 units in a symmetrical arrangement. In complex 3, each copper ion is coordinated to four oxygen atoms from the carboxylate groups of symmetry-related LHTzdc with $\text{Cu1A} \cdots \text{Cu1B}$ distances of 6.3602(2) Å.

Fig. 2e shows a cross nano-cage, with four ligands forming the side walls and two ligands coordinating to the four $\text{Cu}(\text{II})$ ions. Inside the structure, each $\text{Cu}(\text{II})$ ion is distinctly coordinated to two L5 ligands and two oxygen atoms from two LHTzdc. Interestingly, the two L5 ligands resemble a cross occurring in the interior of the structure, and the crossed coordination motif resembles a “helicite”. Complex 5 shows $\text{Cu1A} \cdots \text{Cu1B}$ distances of 15.6461(6) Å, with an inclination angle ($\text{Rh4} \text{--} \text{Rh1} \text{--} \text{Cu1}$) of 65.363(1)°. Outside of the nano-cage, four L5 ligands are coordinated to eight Cp^*Rh units, similarly generating a right-handed helical mode. Despite many attempts, no incorporation of guest molecules in the cavities of the structures was observed (except for solvent molecules).

In Fig. 2, the release of Febuxostat tablets from the complexes was investigated using a classic transdermal drug release study

with a two-chamber diffusion cell. Except for complex 2, the other four complexes can lead to a significant increase in drug release as compared with the control, which indicates that the interaction between Febuxostat tablets and the complexes for 24 hours is beneficial for drug release. These four complexes play a role in the sustained release of drugs to different degrees, which can effectively reduce the number of times that the drugs need to be taken, reduce the toxicity and side effects of drugs and reduce the total amount of drugs used. Complexes 4 and 5 have better effects; 4 is a linear-type nano-cage with a larger inner cavity and 5 is a screw-type nano-cage. Although the structures of the two compounds are different, the effects are not much different, which shows that all the nano-cage compounds can play a good role in drug delivery.

An *in vitro* skin penetration assay is one way to predict drug penetration *in vivo* and has been validated by *in vitro* correlation studies. The amount of skin penetration in complex 3 was $280 \mu\text{g cm}^{-2}$; the results from the caged drug-loading were the best when the side arms of the caged molecules were longer and there was no cross-coordination in the caged molecules (Fig. 3). The experimental results showed that the drug-loading performance of the compound can be improved by extending the side arm of the molecular cage with divalent copper ions as the center. However, a longer side arm was not better for complex 4 because the side arm of complex 4 is flexible enough to cross-coordinate, and the internal space of the molecular cage is small; the drug-loading effect of complex 5 with the longest side arm is not ideal because the drug-carrying molecules will specifically choose the size of nano-cage and diameter.

The biocompatibility of the complexes with skin was assessed by a non-invasive *in vivo* skin erythema test. As shown in Fig. 4, in the group of 10% SDS, the ΔEI increased significantly, indicating that the skin reacted normally to irritants. The application of the complexes suspended in water did not increase ΔEI , indicating high biocompatibility with skin.

3. Experimental

3.1 Synthesis and characterization of complexes 1–5

3.1.1 Synthesis of complexes 1–5. 1,2,3-triazole-4,5-dicarboxylic acid (LHTzdc) (157 mg, 0.1 mmol) and NaOH

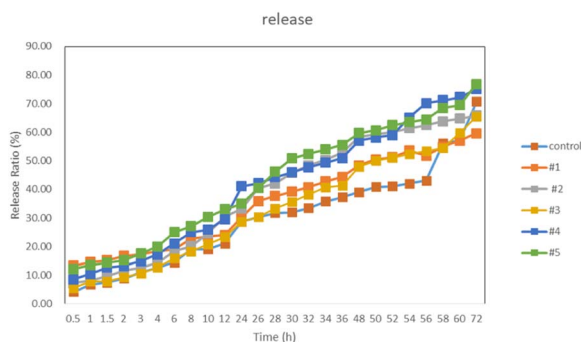


Fig. 2 *In vitro* drug release of Febuxostat tablets with complexes.

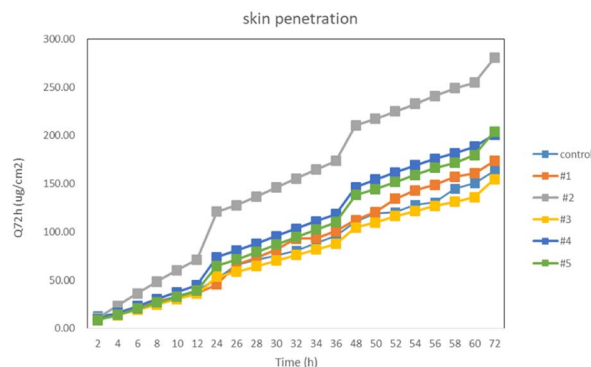


Fig. 3 *In vitro* skin penetration of Febuxostat tablets released from the complexes.



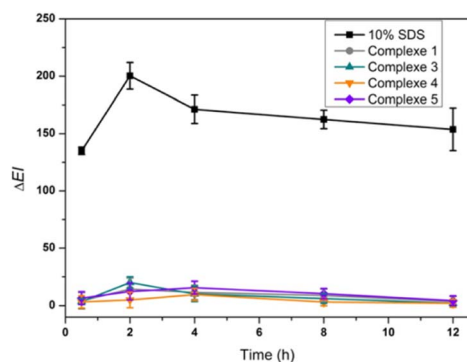


Fig. 4 Biocompatibility of the complexes.

(12.0 mg, 0.3 mmol) or KOH (17.1 mg, 0.3 mmol) were stirred strongly in 10 mL of MeOH at room temperature for 12 h, affording a slight yellow creamy slurry of the sodium salt. The solvent was removed by filtration and the remaining solid was washed with Et₂O (20 mL), followed by the addition of the solution of [Cp*RhCl₂]₂ (61.8 mg, 0.1 mmol), and sodium salt (20.1 mg, 0.1 mmol in 10 mL of MeOH). The metal salt Cu(NO₃)₂·3H₂O (12.1 mg, 0.05 mmol) was then added to the solution. AgOTf (51.2 mg, 0.2 mmol) was stirred in the dark at room temperature for 12 h, and then filtered to remove insoluble materials. After that, L1 (23.4 mg, 0.15 mmol), L2 (27.3 mg, 0.15 mmol), L3 (31.5 mg, 0.15 mmol), L4 (33.8 mg, 0.15 mmol), or L5 (36.3 mg, 0.15 mmol) was added to the mixture. After 12 h of stirring, a yellow-green mixture resulted, and MeOH was evaporated under a vacuum. Crystals of complexes 1–5 that were suitable for an X-ray diffraction study were obtained by the slow diffusion of diethyl ether into a mixture solution in MeOH and CH₃CN (1 : 1).

3.1.2 Characterization of complex 1. Green solid, yield: 89.4%, 114.2 mg. Anal. calcd for C₁₈₂H₃₁₀Cu₄F₁₈N₃₂Na₂O₁₀₉-Rh₈S₆: C, 34.43; H, 4.92; N, 7.06; found: C, 34.66; H, 4.56; N, 7.28; IR (KBr disk): 3649, 3629, 3481, 2923, 1611, 1577, 1529, 1491, 1384, 1274, 1168, 1073, 1032, 937, 820, 785, 640, 576, 518, 454 cm⁻¹.

3.1.3 Characterization of complex 2. Green solid, yield: 88.5%, 127.2 mg. Anal. calcd for C₁₉₄H₂₄₄Cu₄F₃₀N₂₈Na₂O₈₂-Rh₈S₁₀: C, 37.02; H, 3.91; N, 6.23; found: C, 37.31; H, 3.70; N, 6.02; IR (KBr disk): 3447, 1612, 1430, 1384, 1280, 1258, 1224, 1160, 1068, 1031, 1168, 836, 784, 638, 573, 557, 517, 473 cm⁻¹.

3.1.4 Characterization of complex 3. Green solid, yield: 87.1%, 128.9 mg. Anal. calcd for C₁₉₂H₂₄₆Cu₄F₂₄N₄₁NaO₇₂Rh₈S₈: C, 37.85; H, 4.07; N, 9.42; found: C, 37.48; H, 4.24; N, 9.25; IR (KBr disk): 3482, 3132, 2920, 1577, 1552, 1530, 1405, 1354, 1384, 1275, 1224, 1161, 1069, 1030, 937, 782, 652, 638, 613, 454 cm⁻¹.

3.1.5 Characterization of complex 4. Green solid, yield: 85.9%, 130.1 mg. Anal. calcd for C₂₃₄H_{270.4}Cu₄F₃₀K₂N₂₄O_{67.2}-Rh₈S₁₀: C, 42.97; H, 4.17; N, 5.14; found: C, 42.64; H, 4.31; N, 5.39; IR (KBr disk): 3511, 2927, 1659, 1611, 1521, 1501, 1430, 1386, 1344, 1257, 1158, 1100, 1065, 1031, 843, 787, 638, 573, 559, 517, 472, cm⁻¹.

3.1.6 Characterization of complex 5. Green solid, yield: 88.7%, 135.5 mg. Anal. calcd for C₁₈₂H₂₃₂Cu₄F₂₄N₄₄Na₂O₈₂Rh₈S₈: C, 35.35; H, 3.78; N, 9.97; found: C, 35.71; H, 3.48; N, 9.68; IR (KBr

disk): 3447, 1712, 1615, 1582, 1508, 1384, 1333, 1281, 1225, 1212, 1160, 1064, 1030, 837, 788, 639, 574, 556, 517 cm⁻¹.

3.2 In vitro drug release study

Drug-in-adhesive patch with 5% materials and 4% ketoprofen (KP) was prepared using solvent evaporation method. A drug release study was conducted with modified Franz diffusion cells at 32 °C. The patch was pasted on a cellulose membrane and then fixed onto the receptor cell with phosphate buffer solution (PBS, pH 7.4) of 4.5 mL. Samples of 2.0 mL were collected at 0.5, 1, 1.5, 2, 3, 4, 6, 8, 10, 12, 24, 26, 28, 30, 32, 34, 36, 48, 50, 52, 54, 56, 58, 60 and 72 h, and then replaced with the same volume of fresh PBS. The drug concentration was determined by Hitachi HPLC (Tokyo, Japan), which consisted of a pump L-2130, auto sampler L-2200 and UV-detector L-2420 and Waters C18 reversed-phase column (Waters, America) (200 × 4.6 mm, 5 μm). The mobile phase of KP was a mixture of methanol, water and acetic acid solution (60 : 40 : 0.2, v/v), and the pH was adjusted to 6.8 with triethylamine. The column temperature was 40 °C and the flow rate was 1 mL min⁻¹. The wavelength of the detector was set at 260 nm.

A simplified Higuchi equation was used to describe the drug release behavior as follows:

$$R = 200 \frac{Dt^{1/2}}{\pi ch^2} \approx k\sqrt{t} \quad (1)$$

where D and h are the diffusion rate and diffusion length, respectively. The release percent R was plotted against \sqrt{t} , and k is the release rate.

3.3 In vitro skin penetration study

Male Wistar rats (180–220 g, 68 weeks old) were supplied by Liaoning Changsheng (Liaoning, China). All the procedures were performed in accordance with the NIH guidelines for the Care and Use of Laboratory Animals and were approved by the Animal Ethics Committee of Shenyang Medical College. Full-thickness skin was prepared as follows. The hair of the abdomen skin was shaved after the rat was anesthetized with urethane (20%, w/v, 6 mL kg⁻¹, i.p.). Abdomen skin was excised after the rat was sacrificed. The adhering subcutaneous tissues were removed carefully.

The patch was pasted on the stratum corneum and then assembled onto the modified Franz cells. Methods of sample collection and drug concentration determination were the same as for the drug release study, except that sample collection was conducted at 2, 4, 6, 8, 10, 12, 24, 26, 28, 30, 32, 34, 36, 48, 50, 52, 54, 56, 58, 60, 72 h. The cumulative drug skin penetration amount was determined by drug concentration and the volume of the sampling point.

$$Q = \left(\sum_{i=2}^n 2.5C_i - 0.5C_{i-2} \right) / A \quad (i = 2, 4, 6, \dots) \quad (2)$$

where Q is the cumulative skin permeation amount, C_i is the concentration in the receiver compartment at time i and A is the effective diffusion area (1.5 cm²). The cumulative amount permeated from the unit area versus time i was plotted.



3.4 *In vivo* skin erythema study

The experimental method is as follows: Mexameter® (MX 16, Courage & Khazaka Co., Germany) was used to evaluate the biocompatibility of the complexes by measuring the erythema index (EI) of the rabbit skin. Here, a 10% (w/v) aqueous solution of sodium dodecyl sulfate (SDS) was used as the positive control. The dorsal skin of the rabbits was shaved and divided into 5 separate sections (2.5 cm × 2.5 cm). Before the application of 500 μL of PBS, the complexes (10% in PBS), or 10% SDS to their separate sections, the initial EI values were measured as EI0. After 8 h, the solutions were removed and the areas were gently cleaned with cotton wool swabs. The EI_t was measured and ΔEI was calculated (ΔE = EI_t – EI₀). The experiment was performed in quadruplicate.

4. Conclusions

A large number of nano-cages and metallacycles with well-designed N-donor ligands and the LHTzdc ligand have been constructed using a range of central metal atoms. By choosing the template with copper ion as the central metal, we can obtain six-sided compounds, and five kinds of [8 + 4] core sandwich rhodium molecular cages by adjusting the length and rigidity and flexibility. Among these, 1,2,3-triazole-4,5-dicarboxylic acid is located on the upper and lower planes of the cage, and the upper two oxygens chelate with the central metal, and the eight vertices coordinate with the rhodium metal, forming a hexahedral structure in which the side arms of each cage choose linear ligands with different lengths. Because of their different levels of rigidity and flexibility, the cage configuration changes in the form of inclination and cross-coordination. In this way, because the coordination mode of Cu–O bridge makes the compounds have more flexible and changeable coordination behavior and good hardness, various cages with complex structures (various pyridine-based ligands with 6 times the amount of side arms) are formed. The metallasupramolecular assemblies prepared include [8Rh + 4M]-6L heterometallic nano-cages (complexes 1–5). This study demonstrates how the choice of corner metal centers and ligands in the construction of heterometallic supramolecular complexes can influence the geometry and composition of the resulting assemblies. Furthermore, the use of ligands of different lengths leads to nano-cages with different cavity sizes, which may lead to their application in transdermal drug delivery. We are currently exploring other methods of functionalization of these multicomponent nano-cages, and the use of coordination-driven self-assembly to prepare new micro-reactors.

Conflicts of interest

There are no conflicts to declare.

Acknowledgements

This work was supported by National natural science foundation (82003639), 2019 Scientific Research Fund of Shenyang

Medical College (20201004, 20191023), Shenyang Medical College of Science and Technology fund project (20186071), 2018 Provincial Key Research Program Guidance Plan (2018225021), Science Prounicatom Of China (21804093).

References

- 1 J. E. Beves, B. A. Blight, C. J. Campbell, D. A. Leigh and R. T. McBurney, *Angew. Chem., Int. Ed.*, 2011, **50**, 9260–9327.
- 2 D. Fujita, Y. Ueda, S. Sato, N. Mizuno, T. Kumasaka and M. Fujita, *Nature*, 2016, **540**, 563–566.
- 3 Q. F. Sun, J. Iwasa, D. Ogawa, Y. Ishido, S. Sato, T. Ozeki, Y. Sei, K. Yamaguchi and M. Fujita, *Science*, 2010, **328**, 1144–1147.
- 4 M. Li, D. Li, M. O' Keeffe and O. M. Yaghi, *Chem. Rev.*, 2014, **114**, 1343–1370.
- 5 L. L. Dang, T. T. Li, T. T. Zhang, Y. Zhao, T. Chen, X. Gao, L. F. Ma and G. X. Jin, *Chem. Sci.*, 2022, **13**, 5130–5140.
- 6 S. M. Jansze, G. Cecot, M. D. Wise, K. O. Zhurov, T. K. Ronson, A. M. Castilla, A. Finelli, P. Pattison, E. Solari, R. Scopelliti, G. E. Zelinski, A. V. Vologzhanina, Y. Z. Voloshin, J. R. Nitschke and K. Severin, *J. Am. Chem. Soc.*, 2016, **138**, 2046–2054.
- 7 Y. Y. Zhang, Y. J. Lin and G. X. Jin, *Chem. Commun.*, 2014, **50**, 2327–2329.
- 8 Y. Y. Zhang, L. Zhang, Y. J. Lin and G. X. Jin, *Chem.–Eur. J.*, 2015, **21**, 14893–14900.
- 9 Y. F. Han, W. G. Jia, W. B. Yu and G. X. Jin, *Chem. Soc. Rev.*, 2009, **38**, 3419–3434.
- 10 Y. Lu, D. Liu, Y. J. Lin, Z. H. Li, F. E. Hahn and G. X. Jin, *J. Am. Chem. Soc.*, 2021, **143**, 12404–12411.
- 11 H. N. Zhang, W. B. Yu, Y. J. Lin and G. X. Jin, *Angew. Chem., Int. Ed.*, 2021, **60**, 15466–15471.
- 12 S. T. Guo, P. F. Cui, X. R. Liu and G. X. Jin, *J. Am. Chem. Soc.*, 2022, **144**, 5130–5140.
- 13 P. F. Cui, X. R. Liu, Y. J. Lin, Z. H. Li and G. X. Jin, *J. Am. Chem. Soc.*, 2022, **144**, 6558–6565.
- 14 B. Kilbas, S. Mirtschin, T. Riis-Johannessen, R. Scopelliti and K. Severin, *Inorg. Chem.*, 2012, **51**, 5795–5804.
- 15 Y. H. Song, N. Singh, J. Jaehoon, H. Kim, E. H. Kim, H. K. Cheong, Y. Kim and K. W. Chi, *Angew. Chem., Int. Ed.*, 2015, **54**, 1–6.
- 16 H. W. Lee, P. Elumalai, N. Singh, H. Kim, S. U. Lee and K. W. Chi, *J. Am. Chem. Soc.*, 2015, **137**, 4674–4677.
- 17 F. Schmitt, J. Freudenreich, N. P. E. Barry, L. Juillerat-Jeanerret, G. Süss-Fink and B. Therrien, *J. Am. Chem. Soc.*, 2012, **134**, 754–757.
- 18 J. J. Li, L. H. Guo, Z. Z. Tian, S. M. Zhang, Z. S. Xu, Y. L. Han, R. X. Li, Y. Li and Z. Liu, *Inorg. Chem.*, 2018, **57**, 13552–13563.
- 19 H. B. Yang, K. Ghosh, Y. Zhao, B. H. Northrop, M. M. Lyndon, D. C. Muddiman, H. S. White and P. J. Stang, *J. Am. Chem. Soc.*, 2008, **130**, 839–841.
- 20 Y. Sakata, S. Hiraoka and M. Shionoya, *Chem.–Eur. J.*, 2010, **16**, 3318–3325.
- 21 H. B. Wu and Q. M. Wang, *Angew. Chem., Int. Ed.*, 2009, **48**, 7343–7345.



- 22 D. Simond, S. E. Clifford, A. F. Vieira, C. Besnardb and A. F. Williams, *RSC Adv.*, 2014, **4**, 16686–16693.
- 23 X. C. Liu and L. Lin, *Inorg. Chem. Commun.*, 2021, **129**, 108660–108665.
- 24 F. E. Hahn, M. Offermann, C. S. Isfort, T. Pape and R. Fröhlich, *Angew. Chem., Int. Ed.*, 2008, **47**, 6794–6797.
- 25 J. J. Liu, Y. J. Lin and G. X. Jin, *Organometallics*, 2014, **33**, 1283–1290.
- 26 Y. Y. Zhang, Y. J. Lin and G. X. Jin, *Chem. Commun.*, 2014, **50**, 2327–2329.
- 27 M. Schmittel, B. He and P. Mal, *Org. Lett.*, 2008, **10**, 2513–2516.
- 28 M. Fujita, K. Biradha, M. Fujita, S. Sakamoto and K. Yamaguchi, *Angew. Chem., Int. Ed.*, 2001, **40**, 1718–1721.
- 29 A. K. W. Chan, W. H. Lam, Y. Tanaka, K. M. C. Wong and V. W. W. Yam, *Proc. Natl. Acad. Sci. U. S. A.*, 2015, **112**, 690–695.
- 30 L. Zhang, L. Lin, D. Liu, L. Jian, Z. H. Li and G. X. Jin, *J. Am. Chem. Soc.*, 2017, **139**, 1653–1660.
- 31 X. C. Liu and Li. Lin, *Inorg. Chem. Commun.*, 2021, **129**, 108660–108666.
- 32 H. R. Zhang, L. H. Guo, Z. Z. Tian, M. Tian, S. M. Zhang, Z. S. Xu, P. W. Gong, X. F. Zheng, J. Zhao and Z. Liu, *Chem. Commun.*, 2018, **54**, 4421–4424.
- 33 Z. Q. Lei, X. Han, S. E. Border, J. Gallucci, R. Z. Pavlovic and J. D. Badjić, *J. Am. Chem. Soc.*, 2018, **140**, 11091–11100.
- 34 S. R. Peurifoy, J. C. Russell, T. J. Sisto, Y. Yang, X. Roy and C. Nuckolls, *J. Am. Chem. Soc.*, 2018, **140**, 10960–10964.
- 35 T. B. Gao, J. J. Zhang, R. Q. Yan, D. K. Cao, D. Jiang and D. Ye, *Inorg. Chem.*, 2018, **57**, 4310–4316.
- 36 Y. F. Zhang, B. Gui, R. F. Chen, G. P. Hu, Y. Meng, D. Q. Yuan, M. Zeller and C. Wang, *Inorg. Chem.*, 2018, **57**, 2288–2295.
- 37 B. Kilbas, S. Mirtschin, T. Riis-Johannessen, R. Scopelliti and K. Severin, *Inorg. Chem.*, 2012, **51**, 5795–5804.
- 38 S. Hiraoka, Y. Hisanaga, M. Shiro and M. Shionoya, *Angew. Chem., Int. Ed.*, 2010, **49**, 1669–1673.
- 39 X. C. Sun, Z. Z. Cong, S. Y. Wu, Y. Zhang, M. C. Zhu, X. J. Bai, S. Shanmugaraju and P. S. Mukherjee, *J. Mater. Chem. C*, 2022, **10**, 15516–15523.
- 40 H. N. Kim, W. X. Ren, J. S. Kim and J. Yoon, *Chem. Soc. Rev.*, 2012, **41**, 3210–3244.
- 41 Y. Lu, Y. X. Deng, Y. J. Lin, Y. F. Han, L. H. Weng, Z. H. Li and G. X. Jin, *Chem*, 2017, **3**, 110–121.
- 42 D. Tian, Y. Li, R. Y. Chen, Z. Chang, G. Y. Wang and X. H. Bu, *J. Mater. Chem. A*, 2014, **2**, 1465–1470.
- 43 H. N. Zhang, W. B. Yu, Y. J. Lin and G. X. Jin, *Angew. Chem.*, 2021, **133**, 15594–15599.
- 44 N. Jiang, G. Li, W. Che, D. Zhu, Z. Su and M. R. Bryce, *J. Mater. Chem. C*, 2018, **6**, 11287–11291.
- 45 M. Mastalerz, *Angew. Chem., Int. Ed.*, 2010, **49**, 5042–5053.
- 46 C. Viravaux, O. Oms, A. Dolbecq, E. Nassar, L. Busson, C. Mellot-Draznieks, R. Dessapt, H. Serier-Brault and P. Mialane, *J. Mater. Chem. C*, 2021, **9**, 8323–8328.
- 47 S. R. Liu, H. T. Chen, H. X. Lv, Q. P. Qin, L. M. Fan and X. T. Zhang, *Mater. Today Chem.*, 2022, **24**, 100984–100994.
- 48 H. T. Chen, S. R. Liu, H. X. Lv, Q. P. Qin and X. T. Zhang, *ACS Appl. Mater. Interfaces*, 2022, **14**(16), 18589–18599.
- 49 T. Zhang, H. T. Chen, S. R. Liu, H. X. Lv, X. T. Zhang and Q. L. Li, *ACS Catal.*, 2021, **11**, 14916–14925.
- 50 S. R. Liu, H. G. Chen and X. T. Zhang, *ACS Catal.*, 2022, **12**(16), 10373–10383.
- 51 H. Chen, T. Zhang, S. Liu, H. Lu, L. Fan and X. Zhang, *Inorg. Chem.*, 2022, **61**(30), 11949–11958.

